FUDMA Journal of Sciences (FJS)
ISSN online: 2616-1370
ISSN print: 2645 - 2944
Vol. 10 No. 10, May, 2026, pp 269 – 275
DOI: https://doi.org/10.33003/fjs-2026-1010-5506

Unsteady Darcy-Brinkman Axial Flow in a Porous Concentric Annulus: A Semi-Analytical Riemann-Sum Approach

[*1]Jibrin Danjuma Yahaya, [2]Abraham Ayegba Alfa, [1]Raji Muhammed and [3]Abdulsalami Momohjimoh

[1]Department of Mathematics and Statistics, Confluence University of Science and Technology, Osara, Kogi State, Nigeria.
[2]Department of Computer Science, Confluence University of Science and Technology, Osara, Kogi State, Nigeria.
[3]Department of Physics, Confluence University of Science and Technology, Osara, Kogi State, Nigeria.

*Corresponding authors' email: yahayajd@custech.edu.ng
ORCID ID: 0000-0002-3701-1585

ABSTRACT

An unsteady pressure-driven axial flow in a saturated porous concentric annulus is investigated through a semi-analytical Laplace-transform and Riemann-sum framework. The incompressible Newtonian flow is formulated with Brinkman-Darcy resistance, no-slip walls, and a suddenly imposed constant axial pressure gradient. The initial-boundary-value problem reduces, after non-dimensionalization and Laplace transformation, to a modified Bessel equation; closed-form expressions are obtained for the transformed transient velocity, the steady velocity, and the inner- and outer-wall skin frictions. The transient fields are recovered by a rapidly convergent Riemann-sum inversion and are validated against the steady-state solution. The results show that the Darcy number strongly amplifies axial motion and wall shear by weakening porous drag, whereas the radius ratio controls the distribution and sign of the shear response. The velocity grows monotonically from rest toward a single-hump annular profile, while the wall shear is positive at the inner cylinder and negative at the outer cylinder under the adopted radial-derivative convention. Excellent agreement between the Riemann-sum solution and the steady limit confirms the accuracy of the semi-analytical formulation. The model provides a compact benchmark for transient porous annular transport and wall-shear prediction in coaxial engineering systems.

Keywords: Transient Axial Flow, Porous Annulus, Darcy-Brinkman Model, Laplace Transform, Riemann-Sum Inversion, Skin Friction.

INTRODUCTION

Transport of viscous fluids through porous annular passages is fundamental in filtration units, petroleum wells, heat exchangers, porous bearings, catalytic reactors, biomedical ducts, and cooling systems in which the wall shear and transient flow-rate response determine operational safety and efficiency. The mathematical treatment of such flows is rooted in porous-media hydrodynamics and in the correct representation of velocity conditions at fluid-porous interfaces. The role of slip and no-slip conditions at porous/plain-media interfaces was emphasized by Sahraoui and Kaviany (Sahraoui & Kaviany, 1992), while Bear's porous-media formulation remains a principal foundation for modeling momentum transport in saturated matrices (Bear, 2013).

Annular and channel flows in porous environments have attracted sustained attention because curvature, confinement, permeability, and wall constraints interact in a non-trivial way. The early analysis of laminar annular flow with porous walls by Berman (Berman, 1958) revealed the importance of wall permeability in cylindrical geometries. Later developments extended the subject to curved porous channels (Avramenko & Kuznetsov, 2008), unsteady Couette flow in anisotropic porous media (Karmakar, 2021), transient Taylor-Dean flow in composite annuli (Jha & Yusuf, 2022), generalized Couette flow of immiscible fluids in anisotropic porous media (Jaiswal & Yadav, 2024), and second-grade-fluid motion between coaxial porous cylinders (Erdoğan & Imrak, 2007). Recent work has further treated immiscible annular Couette flow in anisotropic porous media (Kumar & Madasu, 2024), start-up flow in channels or pipes saturated with porous media (Avramenko & Kuznetsov, 2009), unsteady Couette flow in composite channels (Jha & Odengle, 2015), hydromagnetic oscillatory slip flow through porous channels (Choudhury et al., 2018), second-grade-fluid flow in porous layers (Masood et al., 2005), transient pressure-driven flow in partially porous annuli (Jha & Yusuf, 2018), dusty-fluid motion in annular-type geometries (Gireesha & Bagewadi, 2012), ramped-pressure-gradient porous-channel flow with slip (Jha & Yunus, 2022), experimental slip-flow behavior at fluid-porous interfaces (K & Sameen, 2015), and sudden application or removal of porous material in generalized Couette flow (Oni et al., 2022). These studies collectively show that permeability modifies momentum diffusion, wall shear, and the time scale over which a transient solution reaches its fully developed state.

Semi-analytical methods remain valuable for such problems because they preserve the governing physics while providing benchmark-quality solutions against which fully numerical calculations can be tested. In annular configurations, Laplace-transform-based approaches have been successfully used to describe transient Dean flow (Jha & Yahaya, 2018), unsteady Dean-flow formation with partial slip (Jha & Danjuma, 2020b), transient flow formation inside annuli (Danjuma, 2019), transient generalized Taylor-Couette flow (Jha & Danjuma, 2020a), transient Dean flow with suction or injection (Jha & Danjuma, 2019), and unsteady Couette flow with variable viscosity (Jha & Danjuma, 2025). These contributions demonstrate that transform methods, when coupled with stable numerical inversion, can accurately capture the early-time flow development and the asymptotic approach to steady state.

The present study revisits unsteady pressure-driven axial flow in a fully porous concentric annulus and rewrites the formulation in a compact, mathematically consistent journal-article form. The principal contributions are: (i) a corrected non-dimensional initial-boundary-value problem for axial flow with linear Darcy-Brinkman resistance; (ii) a closed

Laplace-domain velocity solution expressed through modified Bessel functions; (iii) transient and steady expressions for inner- and outer-wall skin friction; and (iv) a Riemann-sum inversion procedure for computing the time-domain velocity and shear responses. The formulation corresponds to the linear Darcy-Brinkman limit. A quadratic Forchheimer inertial-drag term is not retained; including it would make the governing equation nonlinear and invalidate the present closed-form Laplace-Bessel solution.

MATERIALS AND METHODS

Physical Interpretation and Basic Equations

The physical configuration is a saturated porous concentric annulus bounded by an inner cylinder of radius r_i and an outer cylinder of radiusr_o. The flow is driven in the axial z-direction by a suddenly imposed constant pressure gradient. The velocity field is assumed incompressible, laminar, axisymmetric, fully developed, and unidirectional, so that

$\mathbf{u} = (0,0,w(r,t)), r_i \le r \le r_o, t > 0.$

Under these assumptions, the continuity equation is identically satisfied.

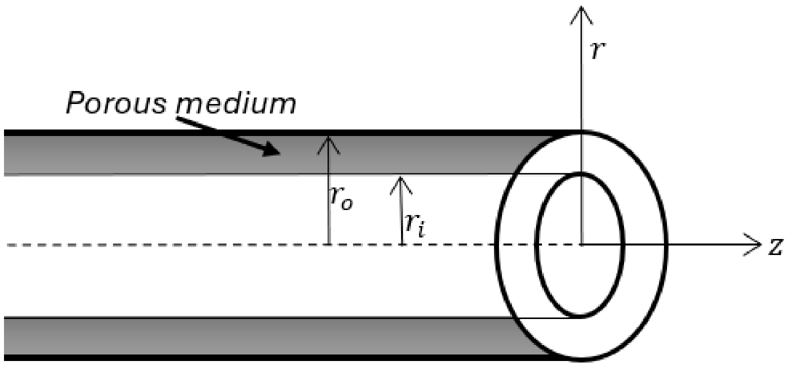

Figure 1: Geometry of the porous concentric annulus and coordinate system.

The axial momentum balance with Brinkman viscous diffusion and Darcy drag is:

$$\rho\frac{\partial w}{\partial t} = -\frac{\partial p}{\partial z} + \mu\left(\frac{\partial^2 w}{\partial r^2} + \frac{1}{r}\frac{\partial w}{\partial r}\right) - \frac{\mu}{K}w, \quad (1)$$

Where ρ is the fluid density, μ is the dynamic viscosity, and p is the pressure. Let the imposed pressure gradient be constant and defined by

$$-\frac{\partial p}{\partial z} = \mathcal{G}, \mathcal{G} > 0. \quad (2)$$

Then equation (1) becomes:

$$\rho\frac{\partial w}{\partial t} = \mathcal{G} + \mu\left(\frac{\partial^2 w}{\partial r^2} + \frac{1}{r}\frac{\partial w}{\partial r}\right) - \frac{\mu}{K}w. \quad (3)$$

The start-up and no-slip conditions are

$$w(r,0) = 0, r_i \le r \le r_o. \quad (4)$$

$$w(r_i,t) = 0, w(r_o,t) = 0, t > 0, \quad (5)$$

The dimensional wall shear stresses are defined by

$$\tau_{r_i} = \mu\left.\frac{\partial w}{\partial r}\right|_{r=r_i}, \tau_{r_o} = \mu\left.\frac{\partial w}{\partial r}\right|_{r=r_o}. \quad (6)$$

Introduce the dimensionless variables:

$$R = \frac{r}{r_o}, \lambda = \frac{r_i}{r_o}, T = \frac{\nu t}{r_o^2}, W(R,T) = \frac{\mu w(r,t)}{\mathcal{G} r_o^2}, \nu = \frac{\mu}{\rho}, Da = \frac{K}{r_o^2}. \quad (7)$$

Where ν is the kinematic viscosity, and λ is the radius ratio, Da is the Darcy number.

The annular domain becomes, $\lambda \le R \le 1$. Substituting Equation (7) into Equation (3) gives the dimensionless governing equation

$$\frac{\partial W}{\partial T} = \frac{\partial^2 W}{\partial R^2} + \frac{1}{R}\frac{\partial W}{\partial R} - \frac{1}{Da}W + 1. \quad (8)$$

The dimensionless initial boundary conditions are:

$$W(R,0) = 0, \lambda \le R \le 1, \quad (9)$$

$$W(\lambda,T) = 0, W(1,T) = 0, T > 0. \quad (10)$$

The dimensionless skin friction used in this work is

$$C_f(R,T) = \frac{\partial W}{\partial R}, C_{f,\lambda}(T) = \left.\frac{\partial W}{\partial R}\right|_{R=\lambda}, C_{f,1}(T) = \left.\frac{\partial W}{\partial R}\right|_{R=1}. \quad (11)$$

Semi-Analytical Solution

Laplace-Domain Velocity Field

Define Laplace in time as (Jha & Danjuma, 2022):

$$\bar{W}(R,\mathcal{S}) = \mathcal{L}\{W(R,T)\} = \int_0^\infty e^{-\mathcal{S}T}\, W(R,T)\, dT. \quad \mathrm{Re}(\mathcal{S}) > 0 \quad (12)$$

Applying Equation (12) to Eqns. (8)-(10), and using the initial condition$W(R,0) = 0$, yields

$$\frac{d^2\bar{W}}{dR^2} + \frac{1}{R}\frac{d\bar{W}}{dR} - \left(\mathcal{S} + \frac{1}{Da}\right)\bar{W} = -\frac{1}{\mathcal{S}}, \quad (13)$$

With

$$\bar{W}(\lambda,\mathcal{S}) = 0, \bar{W}(1,\mathcal{S}) = 0. \quad (14)$$

The associated homogeneous equation is a modified Bessel equation of order zero. Therefore, the transformed solution has the form:

$$\bar{W}(R,\mathcal{S}) = \frac{1}{\mathcal{S}\left(\mathcal{S}+\frac{1}{Da}\right)}\left[1 + \frac{\left\{K_0\left(\sqrt{\mathcal{S}+\frac{1}{Da}}\right) - K_0\left(\lambda\sqrt{\mathcal{S}+\frac{1}{Da}}\right)\right\}I_0\left(R\sqrt{\mathcal{S}+\frac{1}{Da}}\right) + \left\{I_0\left(\lambda\sqrt{\mathcal{S}+\frac{1}{Da}}\right) - I_0\left(\sqrt{\mathcal{S}+\frac{1}{Da}}\right)\right\}K_0\left(R\sqrt{\mathcal{S}+\frac{1}{Da}}\right)}{\left[I_0\left(\sqrt{\mathcal{S}+\frac{1}{Da}}\right)K_0\left(\lambda\sqrt{\mathcal{S}+\frac{1}{Da}}\right) - I_0\left(\lambda\sqrt{\mathcal{S}+\frac{1}{Da}}\right)K_0\left(\sqrt{\mathcal{S}+\frac{1}{Da}}\right)\right]}\right], \quad (15)$$

Where I_0 and K_0 are modified Bessel functions of the first and second kinds of order zero.

Equation (15) follows directly from the modified Bessel equation of order zero. It also satisfies the two no-slip boundary conditions at both $R = \lambda$ and$R = 1$. The transient velocity in the physical time domain is formally

$$W(R,T) = \mathcal{L}^{-1}\{\bar{W}(R,\mathcal{S})\}. \quad (16)$$

Since Equation (15) contains modified Bessel functions of a complex Laplace parameter, the inversion is carried out using the Riemann-sum approximation as earlier described.

Steady Velocity Field

At steady state, $\frac{\partial W}{\partial T} = 0$ and Equation (8) reduces to:

$$\frac{d^2 W_s}{dR^2} + \frac{1}{R}\frac{dW_s}{dR} - \frac{W_s}{Da} = -1. \quad (17)$$

Subject to

$$W_s(\lambda) = 0, W_s(1) = 0, \quad (18)$$

Then the steady solution is:

$$W_s(R) = Da\left[1 + \frac{\left\{K_0\left(\sqrt{\frac{1}{Da}}\right) - K_0\left(\lambda\sqrt{\frac{1}{Da}}\right)\right\}I_0\left(R\sqrt{\frac{1}{Da}}\right) + \left\{I_0\left(\lambda\sqrt{\frac{1}{Da}}\right) - I_0\left(\sqrt{\frac{1}{Da}}\right)\right\}K_0\left(R\sqrt{\frac{1}{Da}}\right)}{I_0\left(\sqrt{\frac{1}{Da}}\right)K_0\left(\lambda\sqrt{\frac{1}{Da}}\right) - I_0\left(\lambda\sqrt{\frac{1}{Da}}\right)K_0\left(\sqrt{\frac{1}{Da}}\right)}\right]. \quad (19)$$

Equation (19) is the large-time limit approached by the transient solution, that is,

$$\lim_{T\to\infty} W(R,T) = W_s(R). \qquad (20)$$

Skin-Friction Formulation

Differentiating Equation (15) with respect to R gives the transformed skin-friction distribution, then the Laplace-domain of the inner- and outer-wall skin frictions are

$$\bar{C}_{f,\lambda}(\mathcal{S}) = \left[\frac{\left\{K_0\left(\sqrt{\mathcal{S}+\frac{1}{Da}}\right)-K_0\left(\lambda\sqrt{\mathcal{S}+\frac{1}{Da}}\right)\right\}I_1\left(\lambda\sqrt{\mathcal{S}+\frac{1}{Da}}\right)-\left\{I_0\left(\lambda\sqrt{\mathcal{S}+\frac{1}{Da}}\right)-I_0\left(\sqrt{\mathcal{S}+\frac{1}{Da}}\right)\right\}K_1\left(\lambda\sqrt{\mathcal{S}+\frac{1}{Da}}\right)}{\mathcal{S}\left(\sqrt{\mathcal{S}+\frac{1}{Da}}\right)\left[I_0\left(\sqrt{\mathcal{S}+\frac{1}{Da}}\right)K_0\left(\lambda\sqrt{\mathcal{S}+\frac{1}{Da}}\right)-I_0\left(\lambda\sqrt{\mathcal{S}+\frac{1}{Da}}\right)K_0\left(\sqrt{\mathcal{S}+\frac{1}{Da}}\right)\right]}\right]. \quad (21)$$

And

$$\bar{C}_{f,1}(\mathcal{S}) = \left[\frac{\left\{K_0\left(\sqrt{\mathcal{S}+\frac{1}{Da}}\right)-K_0\left(\lambda\sqrt{\mathcal{S}+\frac{1}{Da}}\right)\right\}I_1\left(\sqrt{\mathcal{S}+\frac{1}{Da}}\right)-\left\{I_0\left(\lambda\sqrt{\mathcal{S}+\frac{1}{Da}}\right)-I_0\left(\sqrt{\mathcal{S}+\frac{1}{Da}}\right)\right\}K_1\left(\sqrt{\mathcal{S}+\frac{1}{Da}}\right)}{\mathcal{S}\left(\sqrt{\mathcal{S}+\frac{1}{Da}}\right)\left[I_0\left(\sqrt{\mathcal{S}+\frac{1}{Da}}\right)K_0\left(\lambda\sqrt{\mathcal{S}+\frac{1}{Da}}\right)-I_0\left(\lambda\sqrt{\mathcal{S}+\frac{1}{Da}}\right)K_0\left(\sqrt{\mathcal{S}+\frac{1}{Da}}\right)\right]}\right]. \quad (22)$$

The corresponding time-domain are:

$$C_{f,\lambda}(T) = \mathcal{L}^{-1}\{\bar{C}_{f,\lambda}(\mathcal{S})\}, \qquad (23)$$

$$C_{f,1}(T) = \mathcal{L}^{-1}\{\bar{C}_{f,1}(\mathcal{S})\}. \qquad (24)$$

Similarly, differentiating Equation (19) yields the steady skin-friction distribution for both walls as

$$C_{f,\lambda}^{(st)} = \sqrt{Da}\left[\frac{\left\{K_0\left(\sqrt{\frac{1}{Da}}\right)-K_0\left(\lambda\sqrt{\frac{1}{Da}}\right)\right\}I_1\left(\lambda\sqrt{\frac{1}{Da}}\right)-\left\{I_0\left(\lambda\sqrt{\frac{1}{Da}}\right)-I_0\left(\sqrt{\frac{1}{Da}}\right)\right\}K_1\left(\lambda\sqrt{\frac{1}{Da}}\right)}{\left[I_0\left(\sqrt{\frac{1}{Da}}\right)K_0\left(\lambda\sqrt{\frac{1}{Da}}\right)-I_0\left(\lambda\sqrt{\frac{1}{Da}}\right)K_0\left(\sqrt{\frac{1}{Da}}\right)\right]}\right], \quad (25)$$

$$C_{f,1}^{(st)} = \sqrt{Da}\left[\frac{\left\{K_0\left(\sqrt{\frac{1}{Da}}\right)-K_0\left(\lambda\sqrt{\frac{1}{Da}}\right)\right\}I_1\left(\sqrt{\frac{1}{Da}}\right)-\left\{I_0\left(\lambda\sqrt{\frac{1}{Da}}\right)-I_0\left(\sqrt{\frac{1}{Da}}\right)\right\}K_1\left(\sqrt{\frac{1}{Da}}\right)}{\left[I_0\left(\sqrt{\frac{1}{Da}}\right)K_0\left(\lambda\sqrt{\frac{1}{Da}}\right)-I_0\left(\lambda\sqrt{\frac{1}{Da}}\right)K_0\left(\sqrt{\frac{1}{Da}}\right)\right]}\right]. \quad (26)$$

These steady expressions provide reference values for assessing the large-time behaviour of the transient skin-friction solution.

Riemann-Sum Approximation of Laplace Inversion

The inverse Laplace transforms in Eqns. (16) and (23)-(24) are evaluated with a Riemann-sum approximation, a robust inversion technique for transformed solutions containing Bessel functions and complex Laplace arguments (Jha et al., 2026; Yahaya et al., 2025). For a Laplace-domain function $\bar{F}(\mathcal{S})$, where F may represent W, $C_{f,\lambda}$, or $C_{f,1}$, the inversion is approximated by

$$F(R,T) = \frac{e^{\epsilon T}}{T}\left[\frac{1}{2}\bar{F}(R,\epsilon) + \mathrm{Re}\sum_{k=1}^{N} \bar{F}\left(R, \epsilon + \frac{ik\pi}{T}\right)(-1)^k\right], \qquad (27)$$

Here $i = \sqrt{-1}$, N is the truncation level, and $\epsilon > 0$ is a convergence parameter that shifts the Bromwich contour into the right half-plane. In practical computations, $\epsilon T \approx 4.7$ is commonly effective, while N is increased until successive values of $F(R,T)$ are unchanged to the prescribed numerical tolerance. The strength of Equation (27) is that it avoids explicit eigenvalue calculations and directly uses the closed Laplace-domain velocity and shear functions. Consequently, the method is well suited to transient annular problems where the geometry naturally leads to modified Bessel functions.

RESULTS AND DISCUSSION

The semi-analytical solution is used to examine the effects of the dimensionless time T, Darcy number Da, and radius ratio λ on the axial velocity and wall-shear response. The curves in Figures 2-7 are obtained from the Riemann-sum approximation, while Tables 1 and 2 compare transient Riemann-sum values with their corresponding steady-state limits. The discussion follows the radial-derivative convention in Equation (11), so that positive shear is expected at the inner wall and negative shear at the outer wall.

Figure 2 displays the transient build-up of the axial velocity for $Da = 1.0$. At all times, the no-slip boundary conditions force $W = 0$ at both walls, while the interior evolves into a single-hump annular profile. As T increases from the early start-up stage to $T = 0.20$, the velocity rises monotonically and the successive curves become more closely packed, indicating progressive saturation toward the steady solution. The maximum velocity occurs near the central annular region, approximately around $R = 0.55 - 0.60$, because the pressure force accelerates the fluid away from the walls while the two no-slip boundaries maintain strong velocity gradients. This behavior agrees with the structure of exact and limiting annular-flow solutions (Sarkar & Biswas, 2021) and with the known axial-flow response in annular configurations (Lueptow et al., 1992; Wereley & Lueptow, 1999).

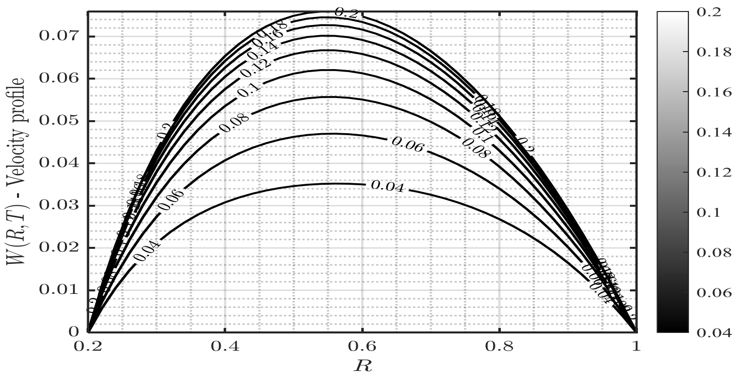

Figure 2: Effect of dimensionless time (T) on the velocity profile for $Da = 1.0$.

Figure 3 shows the influence of the Darcy number on the velocity field at fixed $T = 0.02$. Increasing Da increases the permeability of the porous matrix and weakens the resistance term $Da^{-1}W$ in equation (8). Consequently, more of the imposed pressure work is converted into axial motion, and the velocity level increases throughout the annulus. The scale of the ordinate, 10^{-3}, confirms that the response is still in the early transient regime; nevertheless, the effect of permeability is already clearly visible. The trend is consistent with porous annular solutions in which permeability reduces drag and amplifies the velocity distribution (Yadav et al., 2020).

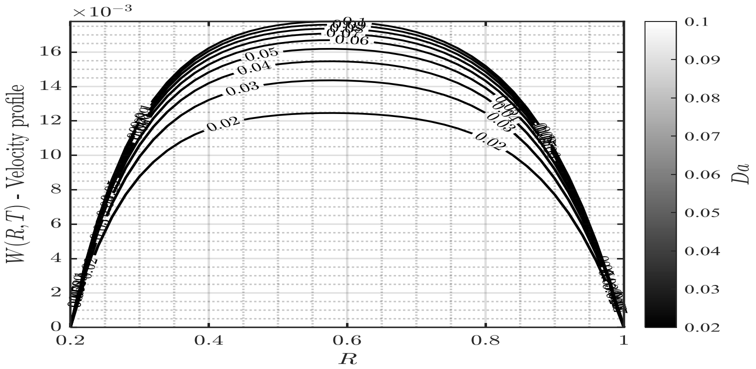

Figure 3: Effect of Darcy Number (Da) on the Velocity Profile for fixed$T = 0.02$.

Figures 4 and 5 quantify the time dependence of wall skin friction at the inner and outer cylinders for$Da = 1.0$. The inner-wall skin friction is positive because W rises from zero at $R = \lambda$ into the annular core. Conversely, the outer-wall skin friction is negative because W falls from the core value back to zero at$R = 1$. These opposite signs are therefore not contradictory; they are a direct consequence of the adopted radial coordinate and the no-slip constraints. With increasing T, both the positive inner-wall shear and the magnitude of the negative outer-wall shear increase, especially for smaller λ where the annular gap is wider and the velocity has more radial space to develop. The time-dependent shear structure is compatible with transient annular-flow theory (Sarkar & Biswas, 2021) and with wall-gradient behavior observed in axial annular configurations (Lueptow et al., 1992; Wereley & Lueptow, 1999).

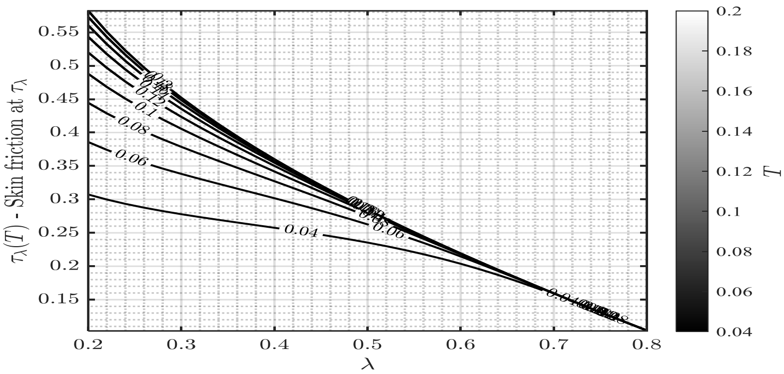

Figure 4: Effect of Dimensionless Time (T) on the Skin Friction at $R = \lambda$ for$Da = 1.0$.

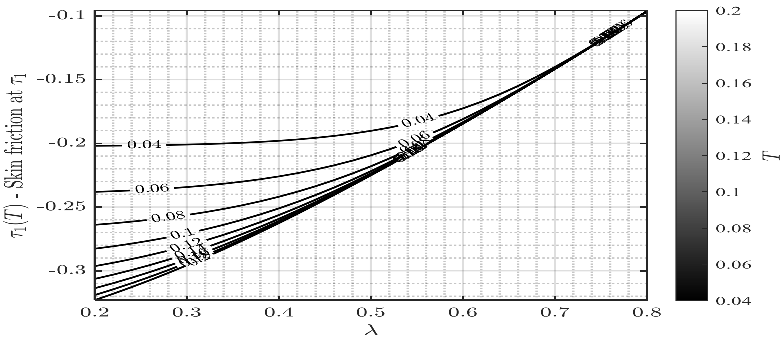

Figure 5: Effect of Dimensionless Time (T) on the Skin Friction at $R = 1$ for$Da = 1.0$.

Figures 6 and 7 show the permeability effect on wall shear at fixed$T = 0.02$. At the inner wall, larger Da increases $C_{f,\lambda}$ because weaker porous drag permits stronger momentum penetration and a steeper near-wall velocity gradient. At the outer wall, larger Da makes $C_{f,1}$ more negative, which means that the magnitude of the outer-wall shear increases. The curves converge as λ approaches 0.8, showing that when the gap becomes narrow the wall constraints dominate the permeability effect. These trends are consistent with analytical porous annular-region results (Yadav et al., 2020) and with recent semi-analytical transient shear predictions in related annular Dean-flow configurations (Basant & Yahaya, 2026).

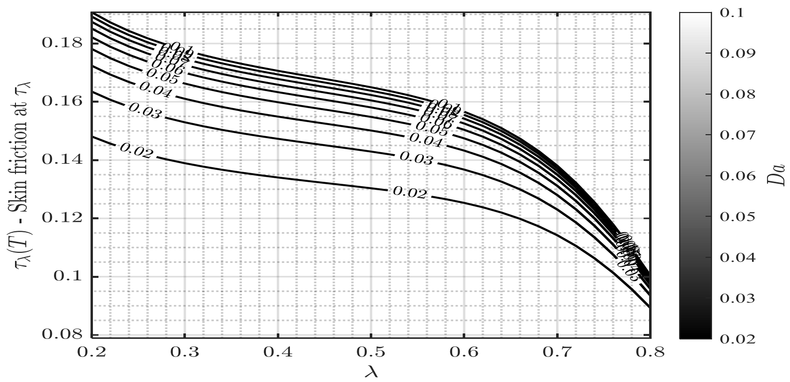

Figure 6: Effect of Darcy Number (Da) on the Skin Friction at $R = \lambda$ for Fixed$T = 0.02$.

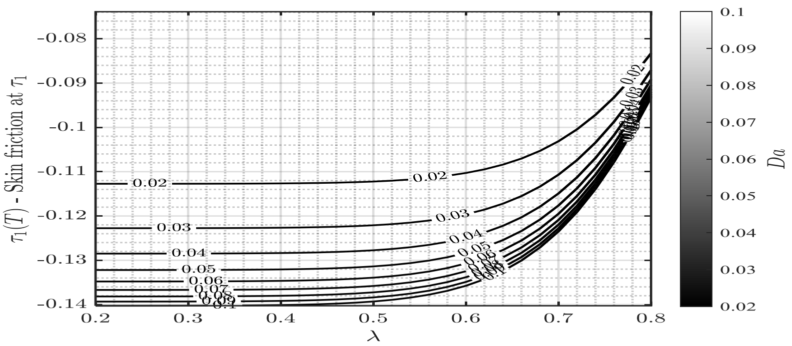

Figure 7: Effect of Darcy Number (Da) on the Skin Friction at $R = 1$ for Fixed$T = 0.02$.

Table 1 confirms the convergence of the Riemann-sum approximation to the steady-state velocity. For$Da = 0.1$, the difference between the RSA and steady-state values is already small at$T = 0.2$; for example, at$R = 0.6$, the velocity changes from 0.0485 to the steady value 0.0489. At$T = 0.4$, the RSA values are essentially identical to the steady values to four significant figures. For$Da = 1.0$, the same convergence is observed, although the transient value at $T = 0.2$ remains slightly farther from the steady limit because the higher permeability permits a larger final velocity. The steady velocity at $R = 0.6$ increases from 0.0489 for $Da = 0.1$ to 0.0783 for$Da = 1.0$, an increase of about 60%, demonstrating the strong role of permeability in pressure-driven porous annular flow.

Table 1: Numerical Values of Axial Velocity Computed by the Riemann-Sum Approximation (RSA) and the Steady-State Solution for Selected Values of$T$,R, and Da

Velocity profile					
		$Da = 0.1$		$Da = 1.0$	
T	R	RSA	Steady-state	RSA	Steady-state
0.2	0.4	0.0426	0.0429	0.0654	0.0685
	0.6	0.0485	0.0489	0.0747	0.0783
	0.8	0.0347	0.0349	0.0511	0.0533
0.4	0.4	0.0429	0.0429	0.0684	0.0685
	0.6	0.0489	0.0489	0.0782	0.0783
	0.8	0.0349	0.0349	0.0532	0.0533
10^4	0.4	0.0429	0.0429	0.0685	0.0685
	0.6	0.0489	0.0489	0.0783	0.0783
	0.8	0.0349	0.0349	0.0533	0.0533

Table 2(a,b) gives the corresponding inner- and outer-wall skin frictions. At$\lambda = 0.4$, increasing Da from 0.1 to 1.0 raises the steady inner-wall shear from 0.2838 to 0.3612, an increase of about 27%. Over the same change in permeability, the magnitude of the steady outer-wall shear increases from 0.2129 to 0.2632, or about 24%. At$\lambda = 0.8$, however, the permeability effect is much weaker: the inner-wall steady shear changes only from 0.1008 to 0.1038, and the outer-wall value changes from -0.0936 to -0.0964. This confirms that the radius ratio moderates the permeability effect by controlling the annular gap width and the wall-gradient distribution. The agreement between RSA and steady values at $T = 10^4$ is exact to the tabulated precision, validating the Riemann-sum inversion and the closed-form steady solution.

Table 2: Numerical Values of (A) Inner-Wall and (B) Skin Frictions $C_{f,\lambda}$, $C_{f,1}$ Computed By RSA and the Steady-State Formula

		(a) Skin friction at $R = \lambda$				**(b) Skin friction at $R = 1$**			
		$Da = 0.1$		$Da = 1.0$		$Da = 0.1$		$Da = 1.0$	
T	λ	RSA	Steady State	RSA	Steady State	RSA	Steady State	RSA	Steady State
0.2	0.4	0.2838	0.2838	0.3601	0.3612	-0.2129	-0.2129	-0.2626	-0.2632
	0.6	0.1955	0.1954	0.2191	0.2190	-0.1659	-0.1658	-0.1845	-0.1844
	0.8	0.1009	0.1008	0.1039	0.1038	-0.0937	-0.0936	-0.0965	-0.0964
0.4	0.4	0.2840	0.2838	0.3613	0.3612	-0.2131	-0.2129	-0.2634	-0.2632
	0.6	0.1956	0.1954	0.2191	0.2190	-0.1660	-0.1658	-0.1845	-0.1844
	0.8	0.1009	0.1008	0.1040	0.1038	-0.0938	-0.0936	-0.0965	-0.0964
10^4	0.4	0.2838	0.2838	0.3612	0.3612	-0.2129	-0.2129	-0.2632	-0.2632
	0.6	0.1954	0.1954	0.2190	0.2190	-0.1658	-0.1658	-0.1844	-0.1844
	0.8	0.1008	0.1008	0.1038	0.1038	-0.0936	-0.0936	-0.0964	-0.0964

Overall, the numerical evidence establishes three central points. First, the transient Riemann-sum solution converges smoothly to the steady analytical solution. Second, permeability intensifies both the velocity and the magnitude of wall shear by reducing Darcy resistance. Third, the radius ratio is a strong geometric control on shear partition: small λ creates a wider annular gap and larger wall-gradient sensitivity, whereas large λ compresses the flow and weakens the influence of permeability.

CONCLUSION

A compact semi-analytical solution has been developed for unsteady pressure-driven axial flow in a saturated porous concentric annulus governed by the linear Darcy-Brinkman model. The governing equation was nondimensionalized correctly and transformed into a modified Bessel boundary-value problem in the Laplace domain. Closed-form expressions were obtained for the transformed transient velocity, the steady velocity, and the inner- and outer-wall skin frictions. The transient solutions were recovered using the Riemann-sum approximation, and the agreement between the Riemann-sum results and the steady-state values confirms the accuracy and stability of the semi-analytical formulation. The results show that the Darcy number is the dominant permeability parameter. Increasing Da weakens the porous-medium resistance, enhances axial momentum transport, increases the velocity profile, raises the positive inner-wall skin friction, and increases the magnitude of the negative outer-wall skin friction. The radius ratio λ controls the annular confinement and therefore regulates the sensitivity of the shear response to permeability. Wider annular gaps exhibit stronger wall-shear sensitivity, whereas narrow gaps suppress permeability-induced variations because the two no-slip walls dominate the flow structure. The present solution provides a reliable benchmark for transient porous annular flows in coaxial engineering systems, including filtration devices, porous bearings, heat exchangers, petroleum-well annuli, catalytic reactors, and biomedical ducts. The findings imply that permeability can be used as an effective control parameter for improving axial transport; however, the associated increase in wall-shear magnitude must be considered in wall-material selection, erosion control, fouling prediction, and the design of porous annular flow devices. Future studies should extend the present linear Darcy-Brinkman model to include true Darcy-Forchheimer nonlinear drag, wall slip, suction or injection, heat transfer, temperature-dependent viscosity, magnetic-field effects, non-Newtonian rheology, and experimentally measured porous-medium properties. In particular, a full Darcy-Forchheimer extension is recommended for high-speed or high-permeability regimes because the quadratic inertial resistance term would make the governing equation nonlinear and would require a nonlinear numerical or iterative semi-analytical solution procedure.

REFERENCES

Avramenko, A. A., & Kuznetsov, A. V. (2008). Flow in a Curved Porous Channel with a Rectangular Cross Section. Journal of Porous Media, 11(3), 241–246. https://doi.org/10.1615/JPorMedia.v11.i3.20

Avramenko, A. A., & Kuznetsov, A. V. (2009). Start-up flow in a channel or pipe occupied by a fluid-saturated porous medium. Journal of Porous Media, 12(4), 361–367.

Basant, J. K., & Yahaya, J. D. (2026). Unsteady magnetohydrodynamic Dean Flow with dynamic as well as static slips. Proceedings of the Institution of Mechanical Engineers, Part E: Journal of Process Mechanical Engineering, 09544089261430086.

Bear, J. (2013). Dynamics of fluids in porous media. Courier Corporation.

Berman, A. S. (1958). Laminar Flow in an Annulus with Porous Walls. Journal of Applied Physics, 29(1), 71–75. https://doi.org/10.1063/1.1722948

Choudhury, R., Deyb, B., & Dasc, B. (2018). Hydromagnetic oscillatory slip flow of a visco-elastic fluid through a porous channel. Chemical Engineering, 71.

Danjuma, Y. J. (2019). Transient Flow Formation inside an Annulus: A Semi-Analytical Approach. In LAP LAMBERT Academic Publishing. https://www.morebooks.de/store/gb/book/transient-flow-formation-inside-an-annulus:-a-semi-analytical-approach/isbn/978-620-0-23920-4

Erdoğan, M. E., & Imrak, C. E. (2007). On the Steady Flow of a Second‐Grade Fluid between Two Coaxial Porous Cylinders. Mathematical Problems in Engineering, 2007(1), 042651.

Gireesha, B. J., & Bagewadi, C. S. (2012). Unsteady flow of a dusty fluid through porous media between annulus of two hexagonal channels. International Journal of Applied Mathematics & Statistics, 27(3), 20–38.

Jaiswal, S., & Yadav, P. K. (2024). Physics of generalized Couette flow of immiscible fluids in anisotropic porous medium. International Journal of Modern Physics B, 38(28), 2450377.

Jha, B. K., & Danjuma, Y. J. (2019). Transient Dean Flow in a channel with suction/injection: A semi-analytical approach. Proceedings of the Institution of Mechanical Engineers, Part E: Journal of Process Mechanical Engineering, 233(5), 1036–1044. https://doi.org/10.1177/0954408919825718

Jha, B. K., & Danjuma, Y. J. (2020a). Transient generalized Taylor-Couette flow: a semi- analytical approach. Journal of Taibah University for Science, 14(1), 445–453. https://doi.org/10.1080/16583655.2020.1745477

Jha, B. K., & Danjuma, Y. J. (2020b). Unsteady Dean flow formation in an annulus with partial slippage: A riemann-sum approximation approach. Results in Engineering, 5, 100078. https://doi.org/10.1016/j.rineng.2019.100078

Jha, B. K., & Danjuma, Y. J. (2022). Transient generalized Taylor–Couette flow of a dusty fluid: A semi-analytical approach. Partial Differential Equations in Applied Mathematics, 5, 100400.

Jha, B. K., & Danjuma, Y. J. (2025). Impact of Variable Viscosity on Unsteady Couette Flow. Heat Transfer, 54(3), 2032–2048. https://doi.org/10.1002/htj.23263

Jha, B. K., & Odengle, J. O. (2015). Unsteady Couette flow in a composite channel partially filled with porous material: A semi - analytical approach. Transport in Porous Media, 107(1), 219–234.

Jha, B. K., & Yahaya, J. D. (2018). Transient Dean Flow in an annulus: a semi-analytical approach. Journal of Taibah University for Science, 13(1), 169–176. https://doi.org/10.1080/16583655.2018.1549529

Jha, B. K., Yahaya, J. D., & Yusuf, T. (2026). Transient generalized Taylor–Couette flow with suction and injection: a semi-analytical approach. Multidiscipline Modeling in Materials and Structures, 1–18.

Jha, B. K., & Yunus, Z. S. (2022). Transient flow through a porous channel with ramped pressure gradient and velocity slip boundary condition. International Journal of Applied Mechanics and Engineering, 27(1), 78–90.

Jha, B. K., & Yusuf, T. S. (2018). Transient pressure driven flow in an annulus partially filled with porous material: Azimuthal pressure gradient. Mathematical Modelling of Engineering Problems, 5(3), 260–267. https://doi.org/10.18280/mmep.050320

Jha, B. K., & Yusuf, T. S. (2022). Transient Taylor—Dean Flow in a composite annulus partially filled with porous material. Thermophysics and Aeromechanics, 29(2), 267–280.

K, A. N., & Sameen, A. (2015). Experimental study of slip flow at the fluid-porous interface in a boundary layer flow. Procedia IUTAM, 15, 293–299. https://doi.org/10.1016/j.piutam.2015.04.041

Karmakar, T. (2021). Physics of unsteady Couette flow in an anisotropic porous medium. Journal of Engineering Mathematics, 130(1), 8.

Kumar, A., & Madasu, K. P. (2024). Annular generalized Couette flow of immiscible viscous fluids in an anisotropic porous medium. Journal of the Brazilian Society of Mechanical Sciences and Engineering, 46(9), 580.

Lueptow, R. M., Docter, A., & Min, K. (1992). Stability of axial flow in an annulus with a rotating inner cylinder. Physics of Fluids A, 4(11), 2446–2558.

Masood, T. H., Ayub, K. M., & Siddiqui, A. M. (2005). The unsteady Couette flow of a second grade fluid in a layer of porous medium. Archives of Mechanics, 57(5), 405–416.

Oni, M. O., Yusuf, A. B., Yusuf, T. S., Adebayo, O. H., & Azeez, L. A. (2022). Unsteady Generalized Couette Flow in a Horizontal Channel with Sudden Application or Removal of a Porous Material. Contemporary Mathematics, 242–256.

Sahraoui, M., & Kaviany, M. (1992). Slip and no-slip velocity boundary conditions interface of porous, plain -media. International Journal of Heat and Mass Transfer, 35(4), 927–943.

Sarkar, U. K., & Biswas, N. (2021). Exact and limiting solutions of fluid flow for axially oscillating cylindrical pipe and annulus. SN Applied Sciences, 3(3), 339.

Wereley, S. T., & Lueptow, R. M. (1999). Velocity field for Taylor–Couette flow with an axial flow. Physics of Fluids, 11(12), 3637–3648.

Yadav, P. K., Puchakatla, J. Y., & Jaiswal, S. (2020). An Analytical Solution of Micropolar-Newtonian Fluid Flow Through Annular Porous Regions. National Academy Science Letters, 43(5), 457–462. https://doi.org/10.1007/s40009-020-00901-7

Yahaya, J. D., Agbata, B. C., Oyeyemi, O. R., Raji, M., Adaji, I., Yusuf, D. A., & Senewo, E. O. (2025). Unsteady dean flow of dusty fluids between two oscillating cylinders. Proceedings of the Nigerian Society of Physical Sciences, 157.